Available online at www.sciencedirect.com
ScienceDirect
Journal of Power Sources 161 (2006) 1002–1011
JOURNAL OF POWER SOURCES
www.elsevier.com/locate/jpowsour

High voltage stability of nanostructured thin film catalysts for PEM fuel cells

Mark K. Debe *, Alison K. Schmoeckel, George D. Vernstrom, Radoslav Atanasoski

3M Fuel Cell Components Program, 201-2N-19, 3M Center, St. Paul, MN 55144, USA

Received 14 March 2006; received in revised form 12 May 2006; accepted 16 May 2006
Available online 11 July 2006

Abstract

This paper provides a comparative evaluation of electrocatalyst surface area stability in PEM fuel cells under accelerated durability testing. The two basic electrocatalyst types are conventional carbon-supported dispersed Pt catalysts (Pt/C), and nanostructured thin film (NSTF) catalysts. Both types of fuel cell electrocatalysts were exposed to continuous cycling between 0.6 and 1.2 V, at various temperatures between 65 and 95 °C, with H_2/N_2 on the anode and cathode, while periodic measurements of electrochemical surface area were recorded as a function of the number of cycles. The NSTF electrocatalyst surface areas were observed to be significantly more stable than the Pt/C electrocatalysts. A first order rate kinetic model was applied to the normalized surface area changes as a function of number of cycles and temperature, and two parameters extracted, viz. the minimum stable surface area, S_{min}, and the activation energy, E_a, for surface area loss in this voltage range. S_{min} was found to be 10% versus 66%, and E_a 23 kJ mole^{-1} versus 52 kJ mole^{-1}, for Pt/C versus NSTF-Pt, respectively. The loss of surface area in both cases is primarily the result of Pt grain size increases, but the Pt/C XRD grain sizes increase significantly more than the NSTF grain sizes. In addition, substantial peak shifts occur in the Pt/C CVs, which ultimately end up aligning with the NSTF peak positions, which do not change substantially due to the voltage cycling. NSTF catalysts should be more robust against shut down/start-up, operation near OCV and local H_2 starvation effects.

Keywords: Polymer electrolyte fuel cells; Electrocatalyst ageing mechanisms; Catalyst surface area stability; Nanostructured thin film catalyst; Catalyst agglomeration; Catalyst support corrosion

1. Introduction

PEM fuel cells are moving steadily towards commercialization for various markets. Needed improvements in performance, durability and cost are becoming better defined, but are generally different for different market opportunities. Operation of PEM fuel cells in the field under real time conditions are expected to reveal further requirements for improvement. The fuel cell membrane electrode assemblies (MEAs) are key to achieving many of these targeted improvements for automotive applications [1], and durability is perhaps the most critical at this stage of technology development. Stability and durability in particular of PEM fuel cell membrane electrode assemblies are known to depend on all the MEA components. Considering just the electrocatalyst electrodes, there are many properties that need to be met simultaneously before a successful system can be implemented. These include high catalyst mass activity, high catalyst utilization at all current densities, low mass transport losses, high tolerance to multiple surface area loss mechanisms, tolerance of a wide humidity and temperature operating window, cold start and freeze tolerance, and the ability to be fabricated by robust high volume-compatible, low cost processes. Specific durability and stability requirements include resistance to corrosion of the catalyst support; stability of surface area against agglomeration, dissolution, and poisoning (externally and internally generated); stability of catalyst surface structure and composition, and negligible peroxide/water ($2e^-/4e^-$) production ratio. Also desirable for MEA durability are resistance of the ion exchange membrane to peroxide attack, low reactant permeability and high dimensional stability; and stability of the gas diffusion layer against carbon oxidation or decomposition that can cause impedance increases and loss of hydrophobicity.

Conventional carbon supported, finely dispersed electrocatalysts, rely on high surface area carbons and 2–3 nm sized catalyst particles on those carbon particles for electrical conductivity and high levels of catalyst activity, respectively. However, these same

* Corresponding author. Tel.: +1 651 736 9563; fax: +1 651 733 0648.
E-mail address: mkdebe1@mmm.com (M.K. Debe).

0378-7753/$ – see front matter © 2006 Elsevier B.V. All rights reserved.
doi:10.1016/j.jpowsour.2006.05.033

Nomenclature

CV	cyclic voltammograms
E_a	activation energy for surface area loss
ECSA	electrochemical surface area
G	pre-exponential constant
GDL	gas diffusion layer
k	Arrhenius rate constant
MEA	membrane electrode assembly
N	number of CV cycles
NSTF	nanostructured thin film catalyst
OCV	open circuit voltage
p	influence parameter in linear regression analysis
Pt/C	Pt on carbon catalysts
PDS	potentiodynamic polarization scan
PEM	proton exchange membrane
PSS	potentiostatic scans
R^2	least squares fitting parameter
S_{min}	minimum normalized surface area

factors contribute to reduced durability from Pt catalyzed electrochemical corrosion of the carbon support itself, and loss of electrochemical surface area (ECSA) due to Pt particle agglomeration and dissolution at high potentials [2–6]. It is generally believed that carbon particle supports, whether carbon blacks, graphitized carbon or carbon nanotubes, are required for adequate electronic conductivity in low catalyst loading PEM fuel cell electrodes. For highly dispersed electrocatalysts on those supports that is true. For a different electrocatalyst structural paradigm however, carbon support particles are not required.

The 3M nanostructured thin film (NSTF) catalyst is such a non-conventional catalyst. Incorporated into an MEA, it contains neither carbon nor additional ionomer in the electrode layers that are 20–30 times thinner than conventional dispersed Pt/carbon based MEAs [7]. Fig. 1 shows SEM images of the NSTF catalyst-coated whiskers, roll-good fabricated by an all-dry continuous process, prior to incorporation onto the surfaces of a PEM to form a catalyst-coated membrane. Fig. 2 shows an SEM cross-section of one side of the catalyst-coated membrane, also fabricated by a dry roll-good process, illustrating the extreme thinness of the electrode layer. The NSTF catalysts comprise high aspect ratio elongated particles formed by vacuum coating catalyst thin films onto a monolayer of oriented crystalline organic (pigment) whiskers [7]. The organic whiskers are highly inert thermally, chemically, and electrochemically [8]. The thin film catalyst coating encapsulates the crystallized pigment whisker support particles, eliminating issues with oxidatively unstable supports. The thin film catalyst coatings consist of relatively large crystallite domains or nanoscopic particles, which give to the NSTF catalysts both enhanced specific activity [9], and resistance to loss of surface area by Pt dissolution [8,10]. Most notable is the five-fold or greater gain in specific activity of the NSTF catalysts over high surface area dispersed Pt/carbon [9,11,12]. We currently associate this fundamental gain in catalyst turn-over rate to be a consequence in

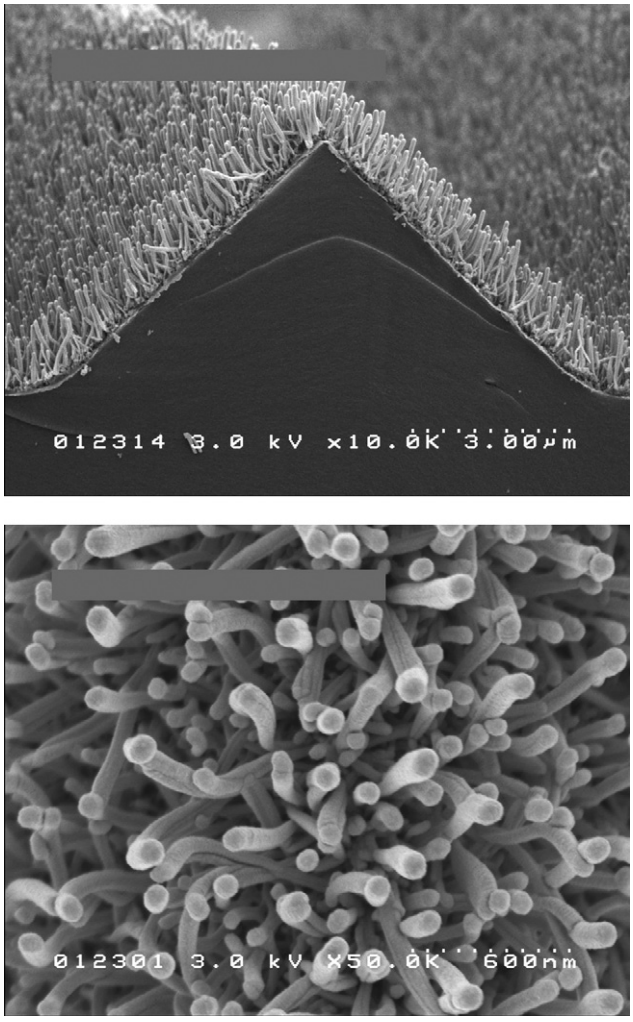

Fig. 1. Scanning electron micrographs of typical NSTF catalysts as fabricated on a microstructured catalyst transfer substrate, seen (top) in cross-section with original magnification of ×10,000, and (bottom) in planview with original magnification of ×50,000. The dotted scale-bar is shown in each micrograph.

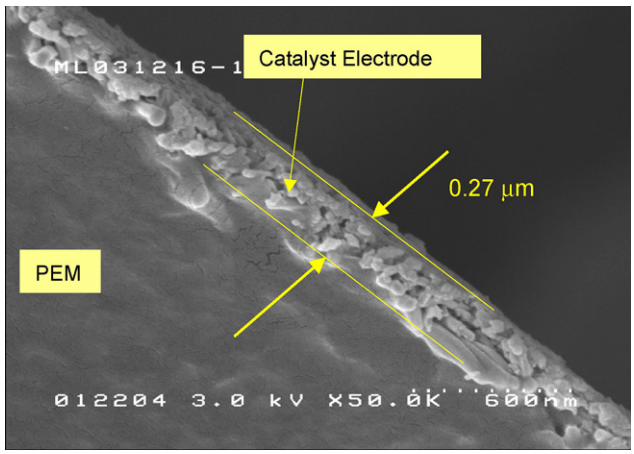

Fig. 2. Scanning electron micrograph of an NSTF catalyst electrode layer after transfer to the surface of the PEM. The cross-sectional view of the catalyst-coated membrane surface at an original magnification of ×50,000 shows the carbon and ionomer free electrode layer thickness is less than 0.3 µm.

some way of the thin film nature of the NSTF catalyst since the absolute values of the specific activity measured in rotating ring disc electrodes agree very well with those from bulk polycrystalline Pt surfaces [11,12]. This gain in specific activity compensates for the lower electrochemical surface area of the NSTF catalysts so that equivalent performances to high surface area carbon supported catalysts are achieved with reduced loadings. Future publications will discuss this unique property in more detail, but by optimizing the surface area of the whisker support to match the volume of the NSTF catalyst over-coating, the mass activities can be made equivalent to the highest values currently attributed to carbon supported dispersed Pt-alloys [1]. But a further critical aspect that enhances the performance of the NSTF electrodes is the extreme thinness of the electrode layer, particularly at high current densities. Because the bulk of the carbon support is eliminated, the NSTF electrode is some 10–30 times thinner than Pt/C based electrodes for the same mass loading of catalyst and this allows for 100% catalyst utilization and reduction of the mass transport overpotential losses at high current densities. As discussed in reference [13], for NSTF electrode thicknesses less than 0.3 μm, corresponding to Pt loadings of 0.10 mg cm^{-2} on the cathode, the mass transport losses under pressurized (303 kPa) H_2/air at 2 A cm^{-2} are deduced to be negligible since IR-corrected polarization curves have linear Tafel slopes of 70 mV $decade^{-1}$ from 0.02 to 2 A cm^{-2}.

The higher specific activity of the NSTF catalysts compared to nano-particle dispersed catalysts, and the absence of exposed carbon also appear to contribute to another very important NSTF property critical for durability. Significantly reduced fluoride ion release rates in the water effluent from NSTF ternary catalyst based MEAs operating at 120 °C show fluoride ion release rates some 75 times lower than from MEAs made with nominally identical membranes and GDLs but conventional Pt/C electrodes. The reduced F^- ion release rates correlated with significantly longer lifetimes, with the NSTF MEAs lasting over 1000 h before catastrophic failure of the PEM versus only about 100 h for the Pt/C based MEAs [11,12].

High voltage stability of the catalyst and its support particle is another key area recently found to uniquely differentiate the NSTF catalysts from conventional carbon-supported dispersed catalysts. The complete resistance of the NSTF to support corrosion at 1.5 V is documented in reference [8] by showing no change in surface area or fuel cell performance occurring over periods as long as 3 h. In sharp contrast, Pt/C catalyst based MEAs with identical membranes and GDLs, exhibited large changes in surface area, performance and ac impedance in just 30 min [8]. The ability of the NSTF catalyst to withstand 1.5 V under H_2/N_2 without corrosion of the support or loss of surface area or loss of catalyst activity, for either pure NSTF Pt or NSTF ternary catalysts, is a significant differentiating feature over carbon or graphitic carbon supported catalysts. In this paper, we compare in more detail the enhanced stability of the NSTF catalysts with respect to Pt dissolution and agglomeration. Surface area and fuel cell performance stability of NSTF-Pt and Pt/C electrocatalysts are compared under accelerated testing conditions of cyclic voltage scanning under H_2/N_2 from 0.6 to 1.2 V at fast rates.

2. Experimental

2.1. Catalyst and MEA preparation

The NSTF catalysts and MEAs were prepared as described in reference [7]. The NSTF whisker support layer is a monolayer of oriented crystalline whiskers of an organic pigment material (CAS #PR149). The support layer is deposited first onto a microstructured catalyst transfer substrate (MCTS) via a vacuum roll-good process. Then catalysts are sputter-coated on top of the whiskers so as to encapsulate them with a polycrystalline thin film. Composition and structure of the catalyst coating is determined by the arrangement and composition of the sputtering targets. Both Pt ternary and pure Pt were used for the NSTF catalysts samples used in this paper to compare with Pt/carbon catalysts for the CV scanning tests. For the first order kinetic rate model data, only pure Pt catalysts were used for both the NSTF and Pt/C MEAs. Typical NSTF Pt loadings were 0.1 and 0.15 mg cm^{-2}, while Pt/C loadings were 0.4 mg cm^{-2} per electrode. The specific surface areas of the NSTF-Pt catalysts were ~10 m^2 g^{-1} Pt. NSTF catalyst-coated membranes are formed by transfer of the catalysts from the initial substrate web (MCTS) to the proton exchange membrane.

For the voltage cycling measurements the dispersed Pt/C catalysts were commercially obtained and utilized 40–50 wt% Pt on Ketjen Black. The specific surface areas of the platinized carbon blacks were ~192 m^2 g^{-1} Pt. Conventional type inks of Pt/C catalysts in Nafion™ were coated and decal-transferred to the surfaces of the membranes to form the dispersed catalyst-coated membranes.

In all cases the 3M fabricated membranes used were based on the 3M ionomer [14]. For the voltage cycling, the 3M membrane having a 1000 EW was used for both the NSTF and Pt/C type MEAs. The same 3M-fabricated GDLs were used for both types of MEAs and generally consisted of a carbon paper electrode backing coated with a microporous layer having a dispersed carbon chosen for its oxidative stability [15].

2.2. Accelerated electrochemical tests

Continuous CV cycling between 0.6 and 1.2 V at 20 mV s^{-1}, with periodic measurements of electrochemical surface area were used to measure the surface area stability of various NSTF and Pt/carbon supported catalysts. To further characterize the surface properties of the catalyst, full-scale CVs were recorded over the voltage range from 0 to 1.2 V.

All the performance fuel cell tests were done in 50 cm^2 cells with quad-serpentine flow fields. Fuel cell performance was obtained on test stations purchased from Fuel Cell Technology, using 3M-developed test station control software. Cyclic voltammograms for surface area determination and voltage cycling were measured using a Solartron 1470 potentiostat controlled by CorrWare software from Scribner Associates.

The high voltage cycling conditions used were 20 mV s^{-1}, with H_2/N_2 at RH: 100%/100% on the anode/cathode, respectively. The temperatures were controlled in the range of

65–95 °C, and a fresh MEA was used for each new temperature condition.

Electrochemical surface areas were measured at room temperature (~22 °C) from integrated hydrogen adsorption and desorption cyclic voltammograms, corrected for shorting and hydrogen cross-over, and assuming 210 μC cm^{-2} of Pt surface area at saturation coverage. For the NSTF catalyst, these CVs were performed at 100 mV s^{-1}, while the Pt/C CVs were at 50 mV s^{-1}.

2.3. X-ray diffraction characterization

X-ray diffraction was used for purposes of determining crystalline phase(s) present, apparent crystallite sizes with high voltage cycling, and semi-quantitative evaluation of the amount of Pt remaining in the MEAs after cycling. Data were collected using a Philips APD vertical diffractometer, copper Kα radiation, reflection geometry, and proportional detector registry of the scattered radiation. The apparent crystallite sizes and d-spacings/relative intensities for platinum were determined from observed diffraction peaks using a Pearson VII peak shape model, accounting for α_1/α_2 separation. The background, obtained from a reference "blank" of Nafion^{TM}, was subtracted prior to profile fitting.

3. Results

Each 50 cm^2 MEA was operated on ambient pressure hydrogen/air with saturated gases until performance had stabilized. The break-in protocol consisted of alternating potentiodynamic scans (PDS) and potentiostatic scans (PSS). Flow rates were held constant at 800 and 1800 sccm of H_2 and air and the cell temperature was held at 75 °C. The PDS ran between 0.85 and 0.25 V in both directions with approximately 48 mV steps and 10 s dwell times at each potential. The PSS were held at 0.4 V for 10 min before another PDS was initiated. For the Pt/C based MEAs, this break-in protocol was continued for approximately 4 h. For the NSTF MEAs, between 2 and 4 additional stop/starts of the fuel cell with cool-down of the cells to ambient temperature was implemented as well, while allowing water to continue to flow through the flow fields. These "thermal cycles" are found helpful to sweep away impurities and bring-up the fuel cell performance of the thin film electrodes more quickly.

For each MEA, after break-in, the initial surface area was measured and then repetitive cyclic voltammograms were acquired between 0.6 and 1.2 V as described in Section 2.2. Periodically the cycling was stopped and the surface area re-measured, after which the CV cycling was continued. This continued until the ECSA dropped below 10% of the initial value (Pt/C MEAs), or until the ECSA stabilized (NSTF MEAs). Since the surface areas of the Pt/C are much greater than that of the NSTF catalysts, to compare ECSA changes it is expedient to normalize the surface areas to the initial values. Fig. 3 illustrates the normalized surface area versus number of CV cycles from 0.6 to 1.2 V for four NSTF catalyst samples and three Pt/carbon catalysts at 80 °C. All MEAs used the same 3M ionomer PEM and GDL. This was a preliminary experiment to get a sense of the magnitude of change depending on the catalyst type and support.

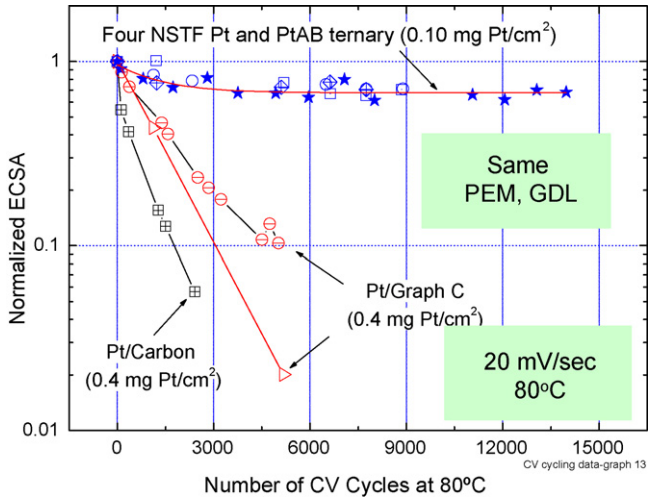

Fig. 3. Normalized surface area vs. number of CV cycles from 0.6 to 1.2 V for four NSTF catalyst samples and three Pt/carbon catalysts at 80 °C. For the NSTF samples, the solid star symbols were pure Pt at 0.15 mg cm^{-2} loading, the open squares were pure Pt at 0.10 mg cm^{-2} loading, the open circles were $Pt_{49}Co_{26}Mn_{25}$ with 0.10 mg Pt cm^{-2}, and the diamond-plus symbols were $Pt_{69}Co_{28}Mn_3$ also with 0.10 mg Pt cm^{-2}. All MEAs used the same 3M ionomer PEM and GDL. The initial mass specific surface areas for the Pt/carbon, Pt-graph-C, and NSTF catalysts were 192, 147, and 10 m^2 (g Pt)$^{-1}$, respectively. (Reproduced from Ref. [8].)

As seen, all the NSTF samples, with both pure Pt and PtCoMn catalysts lost about 30% of the initial surface area after about 3000 cycles, but then the surface area stabilized out to 14,000 cycles. In contrast, the Pt/carbon supported catalysts lost 90% of their surface area in 2000 cycles, and even the Pt dispersed on graphitic carbon supports lost 90% or more of their surface areas in 5000 cycles.

To more carefully study the surface area loss processes for both types of catalysts, a new set of MEAs were evaluated with the same CV cycling protocol but varying cell temperatures. Also, only pure Pt based NSTF catalysts were tested for comparison to the Pt/carbon (Ketjen black) supported catalysts. The NSTF MEAs were tested at 75, 85, 90, and 95 °C while the Pt/C MEAs were tested at 65, 75, 80, 95, and 95 °C. Fig. 4 shows a subset of the CVs obtained at room temperature after cycling at 75 °C from the Pt/C MEAs during a total of 1880 cycles, and NSTF-Pt MEAs during a total of 7226 cycles. Whereas the Pt/C MEA CVs undergo significant changes, the NSTF MEA CVs are much more stable. Pt/carbon peak positions shift dramatically as surface area is reduced by 95% over 1880 cycles at 75 °C, while NSTF CV shape remains nearly unchanged, as surface area is reduced 32% over 7226 cycles. The former shows changes resulting from the considerable loss of surface area and also peak shifts indicated by the red arrows. Fig. 5 shows a similar set of CVs after cycling at 90 °C cell temperature that illustrates a similar behavior as seen at 75 °C. There is again a significant shift in the peak positions for the Pt/C catalysts after 1890 cycles, and a measurable but much smaller shift for the NSTF-Pt CVs after 4235 cycles.

Fig. 6 plots the normalized surface area versus number of cycles for the two catalyst types at all the temperatures measured. A similar response to that seen in the preliminary experiment

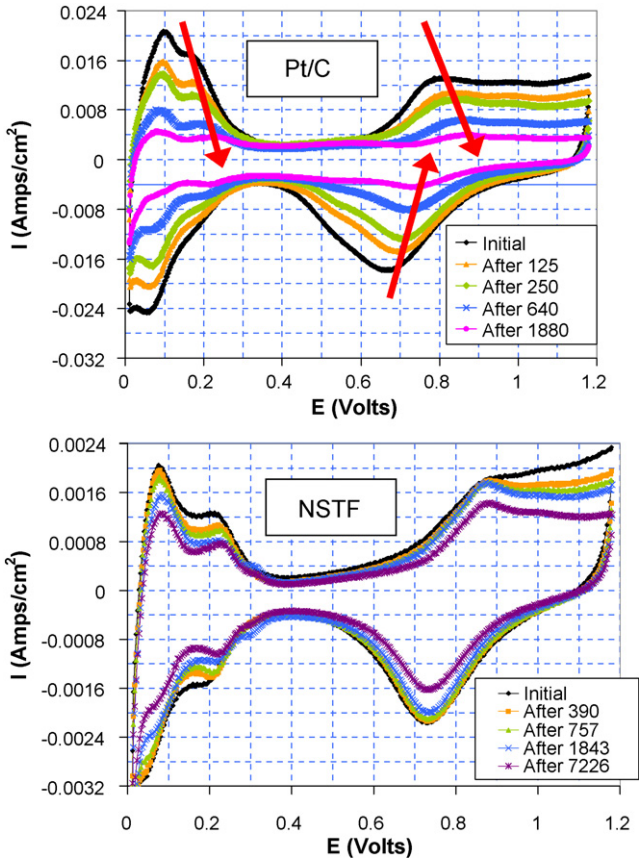

Fig. 4. Series of CV plots obtained at 75 °C during 0.6–1.2 V cycling at 20 mV s^{-1} under H_2/N_2 from (top) Pt/C MEA after 1880 cycles, and (bottom) NSTF MEA after 7226 cycles. CVs were obtained at room temperature (as part of the surface area routine) after CV cycling at 75 °C. The arrows indicate shifts in the Pt/C CV peaks as the surface area is lost.

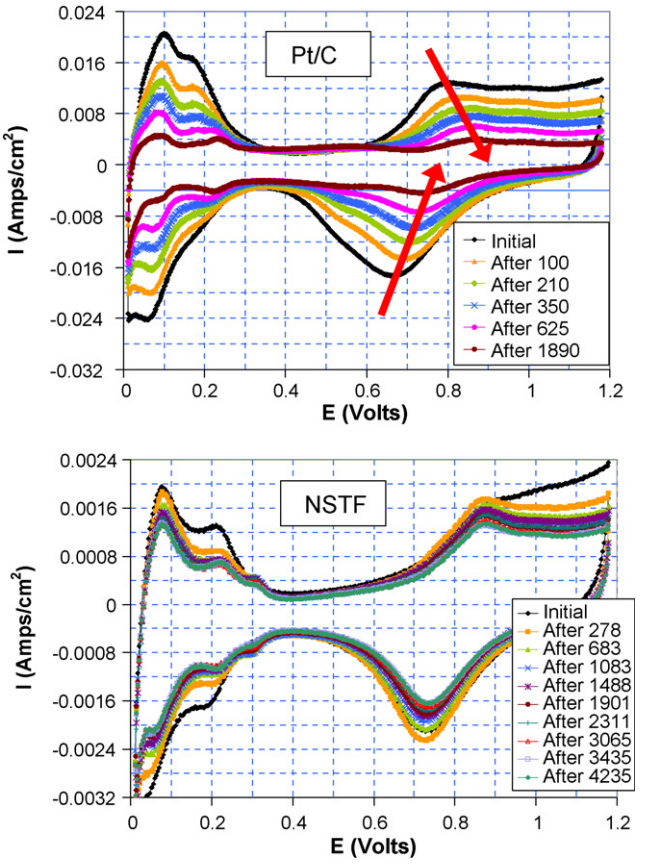

Fig. 5. Series of CV plots obtained at room temperature after 0.6–1.2 V cycling at 90 °C and 20 mV s^{-1} under H_2/N_2 from (top) Pt/C MEA after 1890 cycles, and (bottom) NSTF MEA after 4235 cycles. The arrows indicate shifts in the Pt/C CV peaks as the surface area is lost.

of Fig. 3 was obtained. There appears to be a slight temperature dependence in that the higher the temperature the faster the loss-rate of surface area. Again the NSTF ECSA has stabilized at ~67% for all temperatures after 5000 cycles, while the Pt/C ECSA has decreased by ~90% in 2000 cycles.

Fig. 7 shows a comparison of the initial (top) and final (bottom) full range cyclic voltammograms from the NSTF-Pt based MEAs and Pt/C based MEAs, showing shifts in H_{upd} and Pt oxide formation and reduction peak positions and the shape of the double layer capacitance occurring as surface area was lost. What is remarkable is that on Pt/C the characteristic peak positions shift to become equal to those of the NSTF-Pt, which change very little or none at all. In conjunction with the XRD results discussed below, this suggests that the peak positions are closely tied to particle size, and the size of the Pt/C crystallites are approaching those of the NSTF catalysts. Also, with cycling the Pt/C CVs show a new peak in the double layer region consistent with additional carbon oxidation (quinone–hydroquinone redox peaks around 0.6 V).

Fig. 8 shows a summary of the CV peak positions plotted as a function of the number of cycles for the Pt/C and NSTF-Pt based MEAs. The much larger relative change in CV peak positions of the Pt/C at 75 and 90 °C is clearly seen, and essentially complete after less than 1000 cycles.

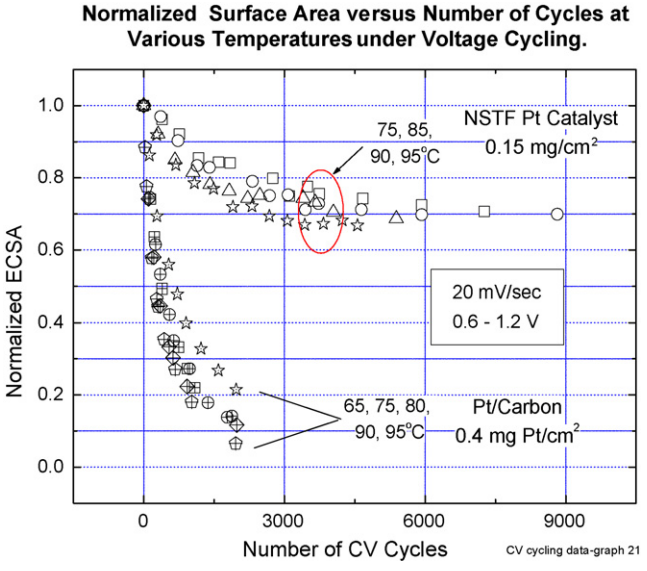

Fig. 6. Normalized catalyst surface area of the working electrode as a function of the number of CV cycles from the NSTF-Pt based MEA (0.15 mg cm^{-2}) at 75 °C (square), 85 °C (circle), 90 °C (star), and 95 °C (triangle), and from the Pt/C based MEA (0.4 mg cm^{-2}) at 65 °C (star), 75 °C (circle), 80 °C (square), 90 °C (diamond), and 95 °C (pentagon).

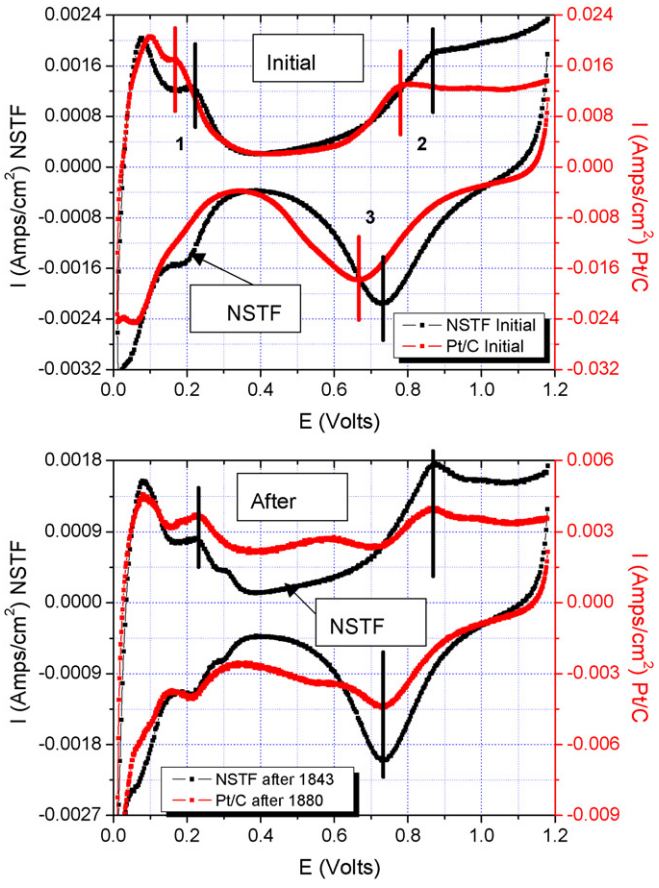

Fig. 7. Comparison of the initial (top) and final (bottom) full range cyclic voltammograms from the NSTF-Pt based MEAs and Pt/C based MEAs, showing shifts in peak positions and double layer capacitance occurring as surface area was lost. Note the change in the current density range for Pt/C between initial and final CVs.

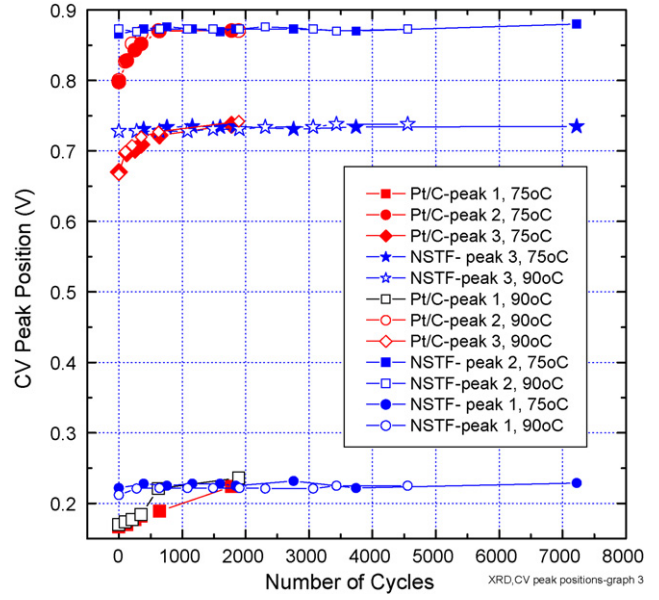

Fig. 8. Summary of the CV peak positions as a function of number of cycles for the Pt/C and NSTF-Pt based MEAs.

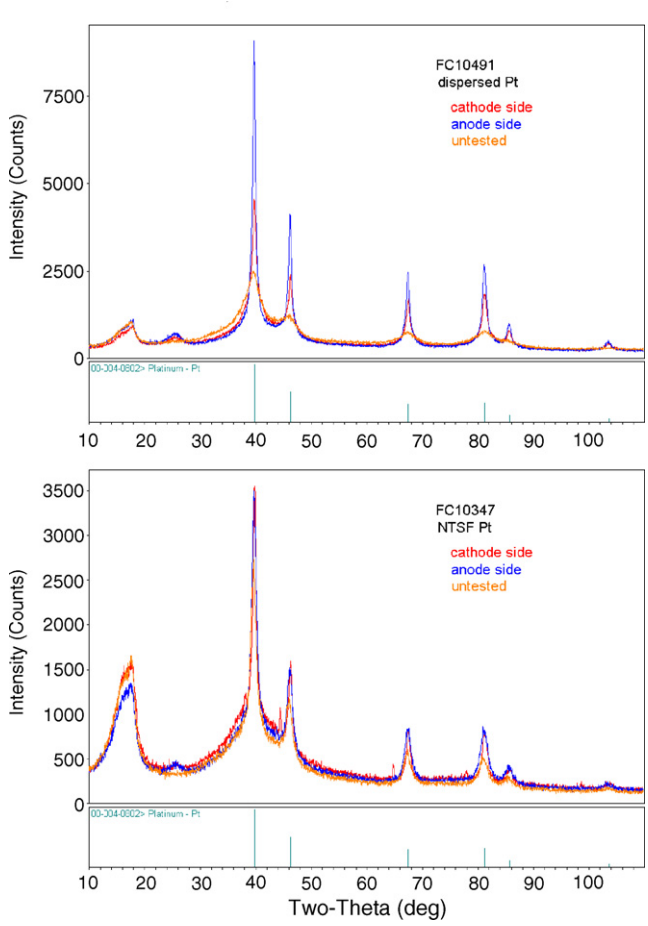

Fig. 9. Comparison of changes in the cathode and anode X-ray diffraction spectra from: (top) the Pt/C based MEAs, and (bottom) the NSTF-Pt based MEAs after 1880 and 7226 CV cycles, respectively.

Fig. 9 compares changes in the cathode and anode X-ray diffraction spectra from the Pt/C based MEAs (top), and the NSTF-Pt based MEAs (bottom). It is readily apparent that the XRD peak widths from the Pt/C electrodes, both anode and cathode, have changed significantly, whereas the NSTF-Pt peak widths have changed much less, and the NSTF-Pt anode peak width hardly at all. The diffraction peak intensities can also be used to qualitatively if not quantitatively address the question of whether loss of ECSA is due to loss of Pt entirely. Table 1 compares the relative integrated peak intensities of the spectra shown in Fig. 9. The values suggest that to within 2%, the integrated peak intensities have not changed as a result of the CV

Table 1
Integrated peak intensities for the XRD spectra shown in Fig. 9

Pt[*h k l*]	Pt/C			NSTF-Pt		
	Untested	Cathode	Anode	Untested	Cathode	Anode
(1 1 1)	100	100	100	100	100	100
(2 0 0)	35	46	42	31	38	33
(2 2 0)	18	37	28	18	23	23
(3 1 1)	22	45	29	15	6	22
(4 0 0)	5	13	8	3	2	6

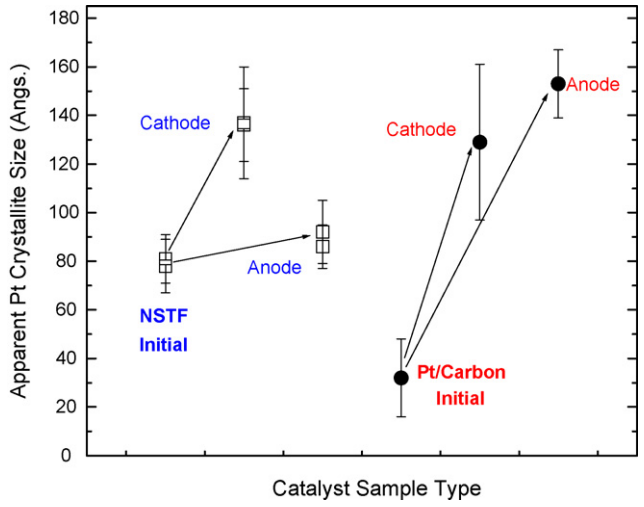

Fig. 10. Changes in the apparent crystallite sizes of the cathode and anode catalysts extracted from the XRD spectra of Fig. 9.

cycling, and the Pt still remains within the CCM, if not within the electrode.

Fig. 10 compares changes in the apparent crystallite sizes of the cathode and anode catalysts, extracted from the XRD spectra of Fig. 9, for the Pt/C based MEA and NSTF-Pt based MEA, after 1880 and 7226 CV cycles, respectively. What is remarkable is that whereas the Pt/C anode crystallites' size increases even more than the cathode crystallites' size, the NSTF anode crystallites' size change very little while the NSTF cathode crystallites' size changes to become very similar to those of the Pt/C. The reason for this is not understood, but was experimentally verified multiple times.

Fig. 11 shows ambient pressure, constant flow PDS polarization curves from the Pt/C based MEA before and after 2429 cycles. The primary loss can probably be attributed to the 90% loss in electrochemically active catalyst surface area. Fig. 12 shows ambient pressure, constant flow PDS polarization curves

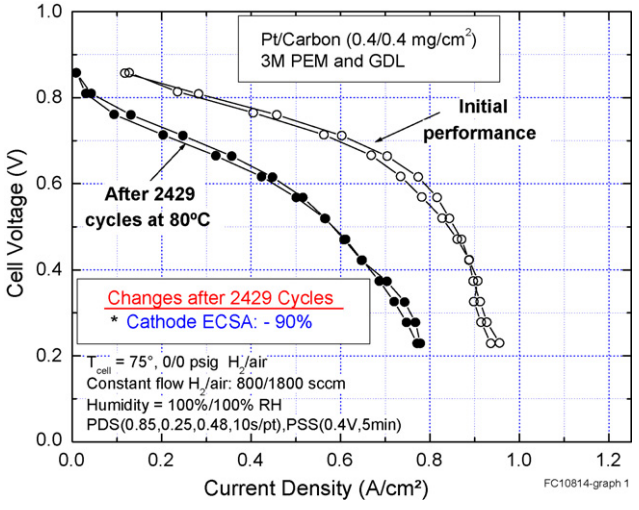

Fig. 11. Ambient pressure constant flow polarization curves from the Pt/C based MEA before and after 2429 cycles. The primary loss can probably be attributed to the 90% loss in electrochemically active catalyst surface area.

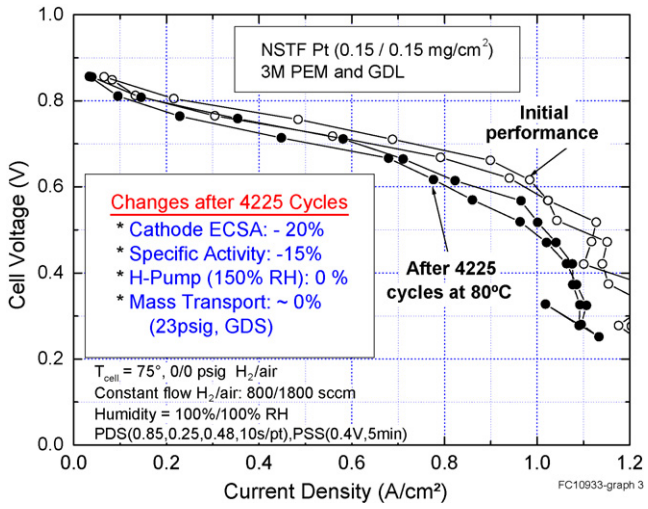

Fig. 12. Ambient pressure constant flow polarization curves from the NSTF-Pt based MEA before and after 4225 cycles. The insert indicates the contributions to the changes in fuel cell performance are due to a ~20% loss of surface area and an ~15% reduction in catalyst specific activity, measured at 900 mV (after 15 min hold) under 100 kPa H_2/O_2 and 100% saturation.

from the NSTF-Pt based MEA before and after 4225 cycles. It is clear from Figs. 11 and 12 that the performance loss due to the CV cycling is much less for the NSTF-Pt MEAs. This performance loss can have contributions from changes in catalyst specific activity, catalyst surface area, overall MEA impedance and mass transport losses. The NSTF MEA impedance was characterized by H-pump measurements in which H^+ transport current across the MEA is measured as a function of applied potential under oversaturated (150% RH) H_2/H_2. The specific activity of the NSTF cathode for the MEA in Fig. 12 was also measured before and after the CV cycling. The measure of specific activity used in this instance was that proscribed by Gasteiger et al. [1]. It consisted of holding the cell at 900 mV under 100 kPa H_2/O_2 and 100% saturation (150 kPa total pressure) and recording the current level after a hold period of 15 min. This current density level, was then corrected for the measured shorting impedance and cross-over current density, and divided by the measured ECSA to obtain the specific activity. Table 2 summarizes the changes in surface area, specific activity and H-pump before and after 4225 CV cycles of the NSTF-Pt sample at 80 °C producing the polarization curves in Fig. 12. No change in the H-pump value occurred before and after CV cycling for the sample, its specific activity was observed to decrease ~15% due to the 4225 cycles, while the surface area was reduced by ~20%. The combination of this loss of surface area and spe-

Table 2
Summary of ECSA, specific activity at 900 mV under 150 kPa H_2/O_2, and H-pump, measured before and after 4225 CV cycles for the NSTF-Pt MEA

NSTF-Pt	ECSA (RT) ($cm^2\ cm^{-2}$) anode/cathode	Specific activity (mA (cm Pt)$^{-2}$)	H-pump ($\Omega\ cm^2$) 150% RH
Before	15.2/13.1	1.72	0.065
After	15.9/10.4	1.44	0.067

cific activity are sufficient to explain the performance change in Fig. 12.

For the Pt/C MEA performance loss in Fig. 11, no attempt was made to characterize changes in mass transport or specific activity due to the very high (~90%) loss of surface area. Qualitative X-ray fluorescence elemental analysis of the untested and tested MEAs of either type showed no statistically significant change in the kilocounts per second due to the CV cycling. This is consistent with the XRD integrated peak intensities in suggesting Pt remains inside of but redistributed within the MEA.

4. First order kinetic rate model for surface area loss

Fig. 6 shows a significant difference in the overall behavior of the Pt/C and NSTF-Pt cathodes. The minimum value of normalized surface area reached after the CV cycling is dramatically different between the two catalyst types. Overall, an exponential type decay of the normalized ECSA is seen for both, which suggests the rate of surface area loss after the Nth cycle is proportional to remaining surface area. Although less obvious, there is also a difference in the rates of surface area loss with temperature, suggesting the kinetics of the surface area loss may be different between the two catalysts types as well. To investigate this, a first order kinetic rate model was applied to the data in Fig. 6. It should be recognized that since the surface area loss can have contributions from multiple specific mechanisms, any activation energy derived from such a model is a composite for all contributing mechanisms to surface area loss from voltage cycling over the range of 0.6–1.2 V.

As a starting basis for the model, the normalized surface area, $S(N)$, is considered to be a function of the number of cycles, N, and after any given number of cycles, N, the rate of surface area loss, $\mathrm{d}S/\mathrm{d}N$, is taken as directly proportional to the remaining losable-surface area, S, as in Eq. (1). The constant of proportionality, k, is a rate constant having the typical Arrhenius dependence on temperature and activation energy, E_a:

$$\frac{\mathrm{d}S}{\mathrm{d}N} = -kS(N), \quad \text{where } k \equiv G\exp^{-E_a/RT}. \tag{1}$$

Integrating (1) between the expected limits of $0 < S(N) < 1$ should give a plot of $\log[S(N)]$ that varies linearly with N. Fig. 13 shows, however, such a plot is definitely not linear. What is most apparent in Fig. 6 is that the NSTF-Pt electrodes have a minimum normalized surface area that is considerably larger than that of the Pt/C. In other words, there appears to be a minimum surface area, S_{min}, which is either stable or much less susceptible to loss by the voltage cycling, so that there is a maximum of normalized losable-surface area of $1 - S_{min}$. With that assumption, the integration limits of Eq. (1) are taken between $1 - S_{min}$ and $S(N) - S_{min}$, giving:

$$\ln\left[\frac{S - S_{min}}{1 - S_{min}}\right] = -kN = -G(\exp^{-E_a/RT})N \tag{2}$$

Fig. 14 is a plot of the left half of Eq. (2) with the value of $S_{min} = 0.10$ for the Pt/C data from Fig. 6. The lines are now substantially linear for all temperatures. A single value of 0.10 for S_{min} was found to give the observed fit for all the temperatures,

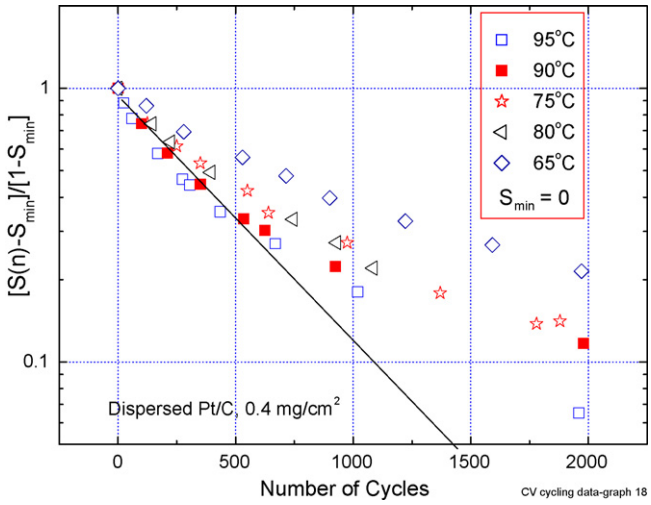

Fig. 13. Plot of the log of the normalized surface area, $S(N)$, from the Pt/C based MEA data shown in Fig. 6 as a function of the number of CV cycles. $S'(N) = [(S(N) - S_{min})/(1 - S_{min})]$ when $S_{min} = 0$.

although a value of 0.12 did improve the R^2 fit value for the $T = 65\,^{\circ}\mathrm{C}$ case.

Fig. 15 shows the results of the left half of Eq. (2) for the NSTF-Pt data from Fig. 6. In this case a single value of S_{min} did not work satisfactorily for each temperature. The values of S_{min} which produced the best linear fits to the data in Fig. 6 for each temperature, as determined by the minimum value of R^2, were in the range shown of $0.64 < S_{min} < 0.69$. Small differences in the value of S_{min} for the NSTF case have a greater impact on the curvature of the plotted lines in Fig. 15 compared to those in Fig. 12 for the Pt/C case because the size of the signal (maximum loss of surface area) is less for the NSTF case (32% versus 90%). Also, the noise is contributed to since the absolute errors in S_{min} are counted twice in the plotted ordinate of Figs. 14 and 15. For example, if the absolute uncertainty in S_{min} is 3% and that of $S(N)$ is 10%, then the fractional uncertainty in $[S(N) - S_{min}]/[1 - S_{min}]$ is 23%. With the model assumptions

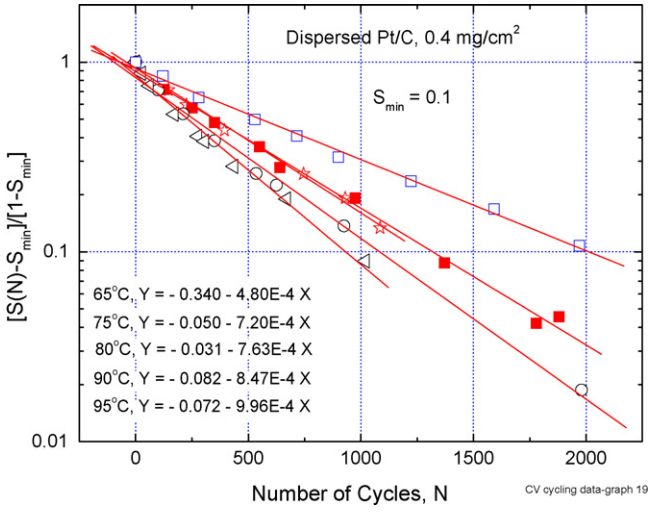

Fig. 14. Plot of the log of (normalized surface area—S_{min},) from the Pt/C based MEA data shown in Fig. 6 as a function of the number of cycles, when $S_{min} = 0.1$.

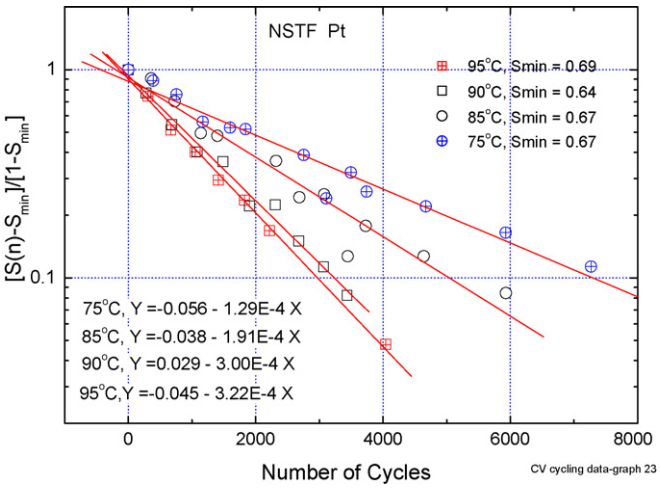

Fig. 15. Plot of the log of (normalized surface area—S_{min},) from the NSTF-Pt based MEA data shown in Fig. 6 as a function of the number of cycles, when $0.64 < S_{min} < 0.69$ is selected for each temperature so as to give the straight line with the least R^2 fit.

that a first order rate equation is applicable and the data plotted in Fig. 13 should be linear, the exact value of S_{min} was allowed to vary in the range of 0.64–0.69 for the NSTF-Pt case in order to obtain best-fit straight lines. Doing so generally gave R^2 values > 0.98, and $p < 0.0001$.

From the slopes of the linear fits to the data in Figs. 14 and 15, the values of the rate constants, $k(T)$, are obtained at each temperature, T. By Eq. (3) plotting $\ln[k]$ versus $1/T$ should also produce a linear fit the slope of which the activation energy, E_a can be obtained:

$$\ln[k] = \ln(G) - \frac{E_a}{R(1/T)} \quad (3)$$

Fig. 16 shows the resulting plots of Eq. (3) for the values of $k(T)$ from Figs. 14 and 15. The overall activation energy, for all possible surface area loss mechanisms taken together, are $E_a = 52.8 \pm 8\,\text{kJ mole}^{-1}$ for the NSTF-Pt electrodes, and $E_a = 22.6 \pm 3.6\,\text{kJ moles}^{-1}$ for the Pt/C electrodes. The uncertainties in these values are the RMS deviation of the linear fits from the data shown in Fig. 16.

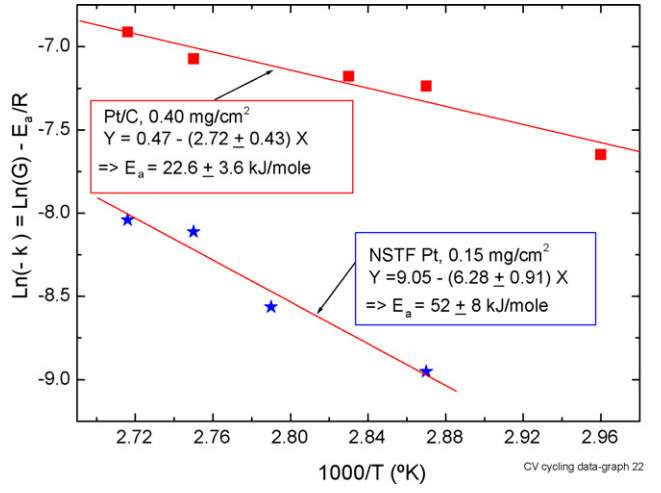

Fig. 16. Arrhenius plot of the linear slopes of the fitted lines from Figs. 8 and 9 as a function reciprocal temperature.

5. Conclusions

NSTF-Pt catalysts (0.15 mg Pt cm^{-2}) are much more resistant to loss of surface area from high voltage cycling than are Pt/carbon (Ketjen Black) with 0.4 mg Pt cm^{-2} loading. The NSTF-Pt asymptotically approaches a maximum of ~33% surface area loss in 9000 cycles, while the Pt/C loses ~90% of the initial surface area in 2000 cycles. The activation energy for surface area loss is twice as high for NSTF (52 kJ mole^{-1} versus 23 kJ mole^{-1}) reflecting a slower rate of surface area loss for NSTF. The NSTF surface area is therefore more stable due to two effects, the higher value of S_{min} and the slower rate of approach to that higher value with number of CV cycles.

The surface area loss in both catalyst types appears to be primarily by agglomeration. Surface Area loss of Pt/C is approximately 90%/2500 cycles, versus only ~20%/4225 cycles for the NSTF-Pt. Both anode and cathode Pt/C crystallite sizes increase 380% and 300%, respectively, but the NSTF crystallite sizes increase only ~10% and 68%, respectively. The thin film nature of the NSTF catalyst is very likely a key property enabling this enhanced stability, over and above that due to the initial larger Pt grain size. By this we mean the catalyst film's metal grains are contiguous and form a conformal layer enshrouding the NSTF whisker core. The NSTF-Pt grains are therefore already highly or even fully agglomerated. The CV cycling may still induce changes in the surface structure or roughness of the contiguous grains, changing the ratio of Pt[*h k l*] facets or defects such as steps and edges of single crystal planes. Such changes may be contributing to the measured changes in both surface area and specific activity of the NSTF catalysts.

The Pt/C dispersed catalyst particles are less stable both because the initial Pt nano-particle diameters are less stable than larger grain sizes, and because they are not contiguous so more Pt atoms can diffuse away from their parent Pt particle or the carbon support particle and become electrochemically inactive. Despite the increased Pt/C particle size, there does not appear to be any increase in catalyst specific activity or catalyst utilization to equal that of the NSTF since the Pt/C polarization curve performance is severely degraded, much more so than the NSTF-Pt.

Fuel cell stack cathodes can experience potentials between OCV under H_2/air (>0.90 V), and OCV under air/air (~1.23 V) during start-up and shut-down, and locally within the active area due to fuel starvation and oxygen cross-over effects. This is observed to lead to serious surface area loss by Pt dissolution and agglomeration [16–18]. Based on the accelerated tests reported above, NSTF catalysts should be more robust against shut down/start-up, operation near OCV and local H_2 starvation effects.

Acknowledgements

The authors would like to acknowledge the 3M Fuel Cell team members Andrew Steinbach, Susan Hendricks, Amy Hes-

ter, Peter Turner, and Paul Kadera for their assistance, and Myles Brostrom and Jason Bender of the 3M Corporate Analytical X-ray Diffraction Laboratory. The work reported here was partially supported by The Hydrogen, Fuel Cells and Infrastructure Technology Program in the Office of Energy Efficiency and Renewable Energy at the US Department of Energy under Cooperative Agreements DE-FC-02-97EE50473, DE-FC02-99EE50582, and DE-FC36-02AL67621.

References

[1] H.A. Gasteiger, S.S. Kocha, B. Sompalli, F.T. Wagner, Appl. Catal. B: Environ. 56 (2005) 9–35.
[2] G. Haugen, D. Stevens, M. Hicks, J. Dahn, Ex-situ and In-situ Stability Studies of PEM Fuel Cell Catalysts: The Effect of Carbon Type and Humidification on the Degradation of Carbon Supported Catalysts, 2005 Fuel Cell Seminar, Palm Springs, CA, November 2005, poster No. 118.
[3] D. Stevens, M. Hicks, G. Haugen, J. Dahn, Ex situ and in situ stability studies of PEMFC catalysts: effect of carbon type and humidification on degradation of the carbon, J. Electrochem. Soc. 152 (12) (2005) A2309.
[4] R.M. Darling, J.P. Meyers, J. Electrochem. Soc. 150 (11) (2003) A1523–A1527;
R.M. Darling, J.P. Meyers, J. Electrochem. Soc. 152 (1) (2005) A242–A247.
[5] L.M. Roen, C.H. Paik, T.D. Jarvi, Electrochem. Solid-State Lett. 7 (1) (2004) A19–A72.
[6] S.D. Knights, K.M. Colbow, J. St-Pierre, D.P. Wilkinson, J. Power Sources 127 (2004) 127–134.
[7] M.K. Debe, in: W. Vielstich, A. Lamm, H.A. Gasteiger (Eds.), Handbook of Fuel Cells—Fundamentals Technology and Applications, John Wiley & Sons, 2003 (Chapter 45).
[8] M.K. Debe, S.M. Hendricks, A.K. Schmoeckel, R.T. Atanasoski, G.D. Vernstrom, G.M. Haugen, Durability aspects of nanostructured thin film catalysts for PEM fuel cells, in: ECS Transactions, vol. 1, Durability and Reliability of Low-Temperature Fuel Cells Systems, 208th ECS Meeting, 2005.
[9] M.K. Debe, A.J. Steinbach, K.A. Lewinski, G.M. Haugen, G.D. Vernstrom, R.T. Atanasoski, A.E. Hester, P.L. Turner, R.J. Ziegler, J.M. Larson, M.T. Hicks, P.E. Serim, Activities of Low Pt Loading Carbon-Less, Ultra-Thin Nanostructured Film-Based Electrodes for PEM Fuel Cells, and Performances in Roll-Good Fabricated MEAs in Single Cells and Stacks, 2003 Fuel Cell Seminar, Miami, FL, November 3–6, 2003.
[10] M.K. Debe, A.K. Schmoeckel, R. Atanasoski, G.D. Vernstrom, Palm Springs, CA, in: High Voltage Stability of NanoStructured Thin Film Catalysts for PEM Fuel Cells, 2005 FC Seminar, November 11–18, 2005.
[11] M.K. Debe, Advanced catalyst and membrane technology with enhanced performance and durability for automotive requirements, in: Proceedings of the 4th International Fuel Cell Workshop 2005, Kofu, Japan, September 22–24, 2005, p. 62.
[12] M.K. Debe et al., VII.A.2 Advanced MEAs for enhanced operating conditions, in: DOE Hydrogen, Fuel Cells and Infrastructure Technologies Program FY 2005 Progress Report, p. 672;
in: DOE Hydrogen Program FY 2004 Progress Report, p. 301.
[13] M.K. Debe, S.M. Hendricks, A.K. Schmoeckel, G.D. Vernstrom, R.T. Atanasoski, P.J. Kadera, A.J. Steinbach, NanoStructured Thin Film, Thin Layer Electrodes Optimized for PEM Fuel Cell Peformance at High Current Density, 2004 Fuel Cell Seminar, San Antonio, TX, November 1–5, 2004.
[14] S.J. Hamrock, The Development of New Membranes for PEM Fuel Cells, Advances in Materials for Proton Exchange Membrane Fuel Cell Systems, Asilomar Conference Grounds, Pacific Grove, CA, February 21, 2005.
[15] J. Frisk, W. Boand, M. Hicks, M. Kurkowski, R. Atanasoski, A. Schmoeckel, MEA Component Durability, 2004 Fuel Cell Seminar, San Antonio, TX, November 1–5, 2004.
[16] C.A. Reiser, L. Bregoli, T.W. Patterson, J.S. Yi, J.D. Yang, M.L. Perry, T.D. Jarvi, Electrochem. Solid-State Lett. 8 (6) (2005) A273–A276.
[17] Y. Ping, P. Marianne, P. Paul, J. Power Sources 144 (2005) 11–20.
[18] W.J. Plieth, J. Phys. Chem. 86 (16) (1982) 3166–3170.